DINAME 2023 - Proceedings of the XIX International Symposium on Dynamic Problems of Mechanics,
A.S. De Paula, A.T. Fabro and M.R. Machado (Editors), ABCM.
Pirenópolis, Go, Brazil, February 26th to March 3rd, 2023

On the Experimental Identification of Jointed Structures: Parametric and Non-Parametric Modeling Perspectives

Rafael Teloli[1], **Gaël Chevallier**[1], **and Samuel da Silva**[2]

[1] FEMTO-ST Institute, Univ. Bourgogne Franche-Comté, UMR CNRS 6174, Department of Applied Mechanics, 24 Chemin de l'épitaphe, 25000 Besançon, France

[2] Universidade Estadual Paulista, Faculdade de Engenharia de Ilha Solteira, Departamento de Engenharia Mecânica, Av. Brasil, 56, Ilha Solteira, 15385-000, SP, Brazil

Abstract: Over the past decades, the scientific community that investigates the dynamics of jointed structures has devoted a significant level of interest in designing tools for new lap-joints configurations, further insights on experimental measurements, proposing reliable predictive models, and developing contributions toward the identification field. In this context, this paper addresses the problem of identifying bolted joints from two points of view. At first, a parametric model, the Duffing-Van der Pol oscillator, is used to represent the nonlinear behavior of an Orion beam. Then, a nonparametric GP-NARX model is approached to reproduce the vibratory response of the BERT benchmark. The advantages and disadvantages of both models in representing the nonlinear behavior of bolted joints are also discussed.

Keywords: Duffing-Van der Pol model, Orion beam, BERT benchmark, GP-NARX, bolted structures

INTRODUCTION

Over the past decades, the scientific community that investigates the dynamics of jointed structures has devoted a significant level of interest in designing tools for new lap-joints configurations, further insights on experimental measurements, proposing reliable predictive models, and developing contributions toward the identification field. The presence of local joints turns the transmission of motion between frictional interfaces into the dominant damping mechanism (Gaul and Nitsche, 2000). The frictional force, which acts in the tangential direction of surfaces in contact, increases monotonically as a function of the vibration amplitude level to which the joint region is subjected. Under these circumstances, an amount of relative tangential slipping (on the order of μm) starts at the interface, known as micro slip. As the vibration amplitude increases, the micro slip progressively becomes the partial slip. These effects that take place on a local scale result in a global nonlinear behavior of the structure. Variations in contact stiffness are seen, as the amount of slip between connected surfaces results in a less stiff system (softening effects), as well as increased damping, when compared to the intrinsic structural damping of the materials.

Note that the nonlinear effects are directly related to the loads imposed in the region around the joints. This implies that not all vibrating modes of a structure will exhibit nonlinear behavior, only those that lead motion in a more pronounced manner at the interface with friction. In this context, this paper addresses the problem of modeling global nonlinear behavior of bolted joint structures from two perspectives: one from physics-based models, and the other from data-driven models.

From the physics-based point of view, a common way to reconstruct the global dynamics of nonlinear modes in bolted structures is through lumped models in the form of single-degree-of-freedom (SDoF) oscillators. In most cases, this class of reduced-order models (ROMs) has discrete nonlinearity terms that are adopted based on a physical understanding (phenomenological approximations) of the source of the nonlinear behavior (Ewins et al., 2015). The restoring force comprises these nonlinear terms, which assume the form of functionals taking into account measurable quantities of motion, such as velocity and displacement[1], to emulate nonlinear phenomena observed in joints, as the presence of multiple harmonics in the response signal, hysteresis on the restoring force $\times$ displacement plane and softening effects. Although formulated in a more simplified way when compared to full finite element models, these models provide a physical insight that enables visualizing, for example, the influence of design choices on the dynamic behavior of bolted joints. Contributions in this context will be addressed by this paper.

Data-driven modeling has gained prominence in structural dynamics applications, especially with the significant advances in machine learning and deep learning tools. In general, data have a qualitative essence and a quantitative extent. Depending on the intended applications in bolted joints, such as for detection of loss of tightening torque in structural health monitoring (SHM) purposes (Miguel et al., 2022), the data to be acquired does not depend exclusively on the physics being addressed, but rather on which purpose it is oriented. In particular, experimentally measured data contain uncertainties, and that makes it possible to quantitatively assess the significance of a difference between measurement and model. In this context, non-parametric models formulated into the Bayesian framework stand out, being an interesting

[1] In practice, due to the availability of measurement instruments, usually one quantity is acquired, either acceleration, velocity, or even displacement, and the others are estimated by numerical integration/derivation.

alternative for applications that require predictive models relying only on input and output data.

To illustrate an application where physics-based models are well suited to explore design choices, the Duffing-Van der Pol model is introduced to evaluate the impact of several tightening torque conditions on the structural stiffness and damping of the Orion beam (Teloli et al., 2022), a structure that suggests an assembly configuration in which there are bolts dedicated to "static" functions to guarantee structural integrity and those that perform "damping" functions to increase the energy dissipation due to frictional contact. In contrast, from a non-parametric point of view, this paper discusses the use of the GP-NARX model to emulate the vibration response of the BERT structure (Teloli et al., 2021b), another bolted joint benchmark (Teloli et al., 2021a), in the presence of uncertainties related to variabilities in the measurement process associated with vibration tests performed on different days.

It is worth mentioning that part of the results presented here, as well as the methodology discussed, were published in recent articles (Teloli et al., 2022, 2021b). However, the present work adopts a different point of view from that already explored in the mentioned publications, offering a parallel and a comparison between the two types of approaches to face the problem of bolted joint identification. In addition to discussing details related to the identification procedure of the Duffing-Van der Pol and GP-NARX models, this paper discusses model-specific details of the excitation design to ensure that both models are able to emulate the vibratory response of the systems under analysis. For covering all these steps, the paper's outline is: section 2 brings forward a general overview on the models investigated by this work. Then, section 3 discusses the characteristics of each model in the context of experimental applications. Finally, section 4 presents the final remarks, as well as a comparison of advantages and disadvantages among the approaches considered by this work.

ON THE MODELING STRATEGIES

Duffing-Van der Pol model

This phenomenological model is used to capture the global nonlinear characteristics observed in a single vibrating mode of bolted structures. In general, in these systems, two main characteristics are noticed in their frequency response curves as the excitation amplitude increases: attenuation of the response amplitude and reduction of the resonance frequencies. Based on the nonlinear amplitude-dependent features observed experimentally in the structure's response, an analytical Duffing-Van der Pol oscillator is considered (Teloli et al., 2022). It is argued that the presence of terms related to both nonlinear damping and nonlinear stiffness can describe the effects of amplitude attenuation and decrease resonance frequencies due to multiple levels of excitation.

The Duffing-Van der Pol oscillator is given by:

$$m\ddot{q}(t) + c\dot{q}(t) + kq(t) + \underbrace{\beta_n \dot{q}(t) q(t)^2}_{\text{nonlinear damping}} + \underbrace{\alpha_n q(t)^3}_{\text{nonlinear stiffness}} = F(t), \tag{1}$$

where m [kg], c [Ns/m] and k [N/m] are the equivalent mass, damping and stiffness coefficients, respectively, whereas β_n [Ns/m^3] and α_n [N/m^3] are coefficients responsible to project the nonlinear restoring forces on physical basis. Considering both the nonlinear terms present in Eq. (1), the parametric model is assumed to be sufficiently general to include the relevant aspects present in the real structure.

The subsequent step within this modeling strategy lies in solving an inverse identification problem to calibrate the model parameters. The methodology adopted in this work consists in using the harmonic balance method to obtain analytical expressions of the oscillator response present in the Eq. (1). This approach is well suited for parametric models with so-called smooth nonlinear forms. By considering a first-order harmonic solution $q(t) = q_s \sin(\Omega t) + q_c \cos(\Omega t)$ for a sinusoidal input $F(t) = F_e \sin(\Omega t)$, one obtains:

$$q(t) = \underbrace{j\left(\mathcal{Q} - \overline{\mathcal{Q}}\right)}_{=q_s} \sin(\Omega t) + \underbrace{\left(\mathcal{Q} + \overline{\mathcal{Q}}\right)}_{=q_c} \cos(\Omega t), \tag{2}$$

where q_s and q_c are the harmonic coefficients, $\mathcal{Q}$ and $\overline{\mathcal{Q}}$ are the fundamental harmonic amplitude and its complex conjugate, respectively, measured at the frequency Ω. This implies that the fundamental harmonic component at the excitation frequency is the most prominent, thus providing a way to capture the main characteristics present in the frequency response curves of nonlinear bolted joints. Substituting equation (2) into equation (1) and balancing the harmonic terms:

$$(-m\Omega^2 + k) q_s - c\Omega q_c - \frac{\beta_n \Omega}{4}\left(q_c^3 - q_c q_s^2\right) + \frac{3\alpha_n}{4}\left(q_s^3 + q_c^2 q_s\right) = F_e, \tag{3}$$

$$(-m\Omega^2 + k) q_c + c\Omega q_s + \frac{\beta_n \Omega}{4}\left(q_s^3 - q_s q_c^2\right) + \frac{3\alpha_n}{4}\left(q_c^3 + q_s^2 q_c\right) = 0. \tag{4}$$

Given equations (3)-(4), the model parameters are estimated by:

$$\left\{\begin{array}{c} m \\ c \\ k \\ \beta_n \\ \alpha_n \end{array}\right\} = \left[\begin{array}{cccc} -\Omega^2 q_s & -\Omega q_c & q_s & \frac{\Omega}{4}\left(q_c^3 - q_c q_s^2\right) & \frac{3}{4}\left(q_s^3 + q_c^2 q_s\right) \\ -\Omega^2 q_c & \Omega q_s & q_c & \frac{\Omega}{4}\left(q_s^3 - q_s q_c^2\right) & \frac{3}{4}\left(q_c^3 + q_s^2 q_c\right) \end{array}\right]^+ \left\{\begin{array}{c} F_e \\ 0 \end{array}\right\}, \tag{5}$$

where $(\bullet)^+$ denotes the pseudo-inverse matrix, the parameters are estimated over each torque condition's excitation band frequency. It is worth mentioning the work of (Jalali et al., 2007), which identified a set of parameters used to describe a nonlinear jointed structure through the harmonic balance framework. However, different from the formulation proposed here, which identifies the whole set of parameters present in the model equation based on harmonic components, (Jalali et al., 2007) considered the nonlinear restoring force's computation for each excitation frequency.

GP-NARX model

A GP regression model is based on the idea of Bayesian inference; however, unlike the inference of the model's parameters used in classic Bayesian regression, the GP model considers the inference directly over functional space (Williams and Rasmussen, 2006). Thus, this model can be described as a generalization of a Bayesian regression method, in which any two or more observations that one wants to describe follow a multivariate Gaussian distribution (Schulz et al., 2018). In this sense, consider a general regression problem to represent the process observations $y_i \in \mathbb{R}$ as

$$y_i = f(\mathbf{x}_i) + \varepsilon_i^{(y)}, \qquad i = 1, 2, \ldots, N \ \text{ samples} \tag{6}$$

where $f(\cdot)$ is a nonlinear function mapping the output to an input $\mathbf{x}_i \in \mathbb{R}^D$, and $\varepsilon_i^{(y)}$ is a stochastic variable representing inherent randomness in the observations. This randomness is assumed to be Gaussian distributed with zero mean

$$\varepsilon_i^{(y)} \sim \mathcal{N}\left(\varepsilon_i^{(y)} | 0, \sigma_y^2\right), \tag{7}$$

where σ_y^2 is the variance of the Gaussian noise observations.

In this work, in order to map the nonlinear effects related to the hysteresis, the NARX structure is considered as a nonlinear function that predicts the output y_i. Thus, the model's input $\mathbf{x}_i$ is formed by regression upon the excitation and output signals

$$\mathbf{x}_i = [y_{i-1}, \ldots, y_{i-n_y}, u_i, u_{i-1}, \ldots, u_{i-n_u+1}]^{\mathrm{T}}, \tag{8}$$

where u_i represents the oscillatory input signal at the i^{th} sample, and n_u and n_y are the number of regressors in the input and output signals, respectively.

Keeping in mind that the regression in equation (6) is represented by a Gaussian Process, the NARX structure $f(\mathbf{x}_i)$ is then formed by the assumption of a multivariate Gaussian prior distribution of zero mean

$$\mathbf{f} = f(\mathbf{x}_i) \sim \mathcal{N}(\mathbf{f}|0, \mathbf{K}), \tag{9}$$

resulting in the so-called GP-NARX model structure, where $\mathbf{K} \in \mathbb{R}^{N \times N}$ is the covariance matrix whose elements are described as $\mathbf{K}_{i,j} = k(\mathbf{x}_i, \mathbf{x}_j)$. The variable $k(\cdot,\cdot)$ is a covariance function, also named a kernel function, that models the dependence between the function values at different input samples. Due to the versatility in the GP-NARX model, the zero mean is assumed for simplicity.

The construction of the model function used for the regression process depends directly on the knowledge acquired about the system of interest. Thus, assuming a set of training data available and making use of a simplified notation, one obtains

$$\mathscr{D} = (\mathbf{x}_i, y_i)_{i=1}^N \equiv (\mathscr{X}, \mathscr{Y}), \tag{10}$$

where $\mathscr{X} \in \mathbb{R}^{N \times D}$ is the regression matrix, and $\mathscr{Y} \in \mathbb{R}^N$ is the output vector. Since data observations for training contribute Gaussian white noise, the joint distribution of the training data and test samples, according to the prior distribution, is given by Williams and Rasmussen (2006)

$$\begin{pmatrix} \mathscr{Y} \\ \mathbf{f}_* \end{pmatrix} \sim \mathcal{N}\left(\begin{pmatrix} \mathscr{Y} \\ \mathbf{f}_* \end{pmatrix} \middle| 0, \begin{bmatrix} \mathbf{K}(\mathscr{X}, \mathscr{X}) + \sigma_y^2 \mathbf{I} & \mathbf{K}(\mathscr{X}, \mathbf{x}_*) \\ \mathbf{K}(\mathbf{x}_*, \mathscr{X}) & \mathbf{K}(\mathbf{x}_*, \mathbf{x}_*) \end{bmatrix}\right), \tag{11}$$

where $\mathbf{f}_*$ denotes the predicted function at new input samples $\mathbf{x}_*$. $\mathbf{K}(\mathscr{X}, \mathscr{X})$ is the covariance matrix computed between the training input samples each other with elements $k(\mathbf{x}_i, \mathbf{x}_j)$, $\mathbf{K}(\mathscr{X}, \mathbf{x}_*)$ is the covariance matrix computed between the training and new input samples with elements $k(\mathbf{x}_i, \mathbf{x}_*)$ and $\mathbf{K}(\mathbf{x}_*, \mathscr{X}) = \mathbf{K}(\mathscr{X}, \mathbf{x}_*)^T$. Finally, $\mathbf{K}(\mathbf{x}_*, \mathbf{x}_*)$ is the covariance matrix between the new input samples and $\mathbf{I} \in \mathbb{R}^{N \times N}$ is an identity matrix.

Then, the Bayesian inference strategy is used to condition a posterior predictive distribution $\pi(\mathbf{f}_*|\mathbf{x}_*,\mathscr{X},\mathscr{Y})$ over $\mathbf{f}_*$ based on the new available input, which gives the main relationship for the GP regression (Williams and Rasmussen, 2006)

$$\pi(\mathbf{f}_*|\mathbf{x}_*,\mathscr{X},\mathscr{Y}) \sim \mathcal{N}(\mathbf{f}_*|\mu_*,\sigma_*^2), \tag{12}$$

where the posterior predictive mean is given by

$$\mu_* = k(\mathbf{x}_*,\mathscr{X})\left[\mathbf{K}(\mathscr{X},\mathscr{X})+\sigma_y^2\mathbf{I}\right]^{-1}\mathscr{Y}, \tag{13}$$

and the posterior predictive variance is given by

$$\sigma_*^2 = k(\mathbf{x}_*,\mathbf{x}_*)-\mathbf{K}(\mathbf{x}_*,\mathscr{X})\left[\mathbf{K}(\mathscr{X},\mathscr{X})+\sigma_y^2\mathbf{I}\right]^{-1}\mathbf{K}(\mathscr{X},\mathbf{x}_*). \tag{14}$$

Using equations (13)-(14), one can predict the new values of the function $\mathbf{f}_*$ as well as the values of $\mathbf{y}_*$ taking into account the model uncertainties, once both predictive distributions are similar. The variance σ_y^2 and the covariance function $k(\cdot,\cdot)$ need to be estimated based on the available data from the system under analysis. Many covariance functions were proposed over the years, with special attention to RBF, Exponential, Matérn 3/2, Matérn 5/2, Polynomial, Rational Quadratic, among others. The choice of the best kernel structure depends on the relations between the input/output data and the previous knowledge available on the system behavior. It is noteworthy that new kernel functions can also be proposed, just by considering a new formulation or even making use of a combination of existing functions (Seeger, 2004). In the context of this work, which explores the application of the GP-NARX model to represent hysteretic systems, the best results were achieved, considering the available data, by selecting a combination of two covariance kernels:

- Matérn 3/2:

$$k_1(\mathbf{x},\mathbf{x}') = \sigma_m^2\left(1+\frac{\sqrt{3}\,|\mathbf{x}-\mathbf{x}'|}{l}\right)\exp\left(-\frac{\sqrt{3}\,|\mathbf{x}-\mathbf{x}'|}{l}\right), \tag{15}$$

  where σ_m is the Matérn kernel variance and l the lengthscale.

- Cubic polynomial:

$$k_2(\mathbf{x},\mathbf{x}') = \sigma_p^2\left[s(\mathbf{x}\mathbf{x}')+b\right]^3, \tag{16}$$

  where σ_p is the Polynomial kernel variance, s the scale and b the bias parameter.

Thus, the new additive kernel is given by

$$k(\mathbf{x},\mathbf{x}') = k_1(\mathbf{x},\mathbf{x}')+k_2(\mathbf{x},\mathbf{x}'). \tag{17}$$

Based on the unknown variables in the kernel, a vector of hyperparameters may be defined as $\boldsymbol{\Theta} = \left[\sigma_m^2, l, \sigma_p^2, s, b, \sigma_y^2\right]$ and then estimated by conducting a maximization of the marginal log-likelihood of the observed data **?**

$$\log\pi(\mathscr{Y}|\mathscr{X},\boldsymbol{\Theta}) = -\frac{1}{2}\log|\mathbf{K}+\sigma_y^2\mathbf{I}| - \frac{1}{2}\mathscr{Y}^{\mathrm{T}}(\mathbf{K}+\sigma_y^2\mathbf{I})^{-1}\mathbf{y} - \frac{N}{2}\log(2\pi). \tag{18}$$

Such a maximization procedure is performed using a gradient method, and the optimum model is used to predict new outputs as a consequence of new inputs. As a result, the GP-NARX model can describe a wide variety of structural dynamic behavior, taking advantage of its capability to consider modeling uncertainties and predicting the trend curves of outputs with probabilistic confidences.

EXPERIMENTAL ASSESSMENT

Description of the experimental setups

Figure 1 is dedicated to introduce the two experimental rigs used for this work. The following subsections describe them in detail.

Orion beam

Figure 1(a) illustrates the Orion beam. The experimental setup consists of a lap-joint structure with dimensions of $370\times30\times2$ [mm], a load cell PCB 288D01, an electromagnetic Modal Shop shaker (Model K2004E01), a 3D scanning laser and a NI9234 hardware for data acquisition. For all measurements, the beam with the contact patches is completely clamped on one side. Notwithstanding, to minimize uncertainties related to the stiffness in the boundary condition, a length of 30 mm is glued and screwed into a massive steel block. The tightening torques applied on the external bolts are 10 cNm, 20 cNm, 30 cNm, and 80 cNm, to observe their influence on the structure's response, whereas the the central bolt

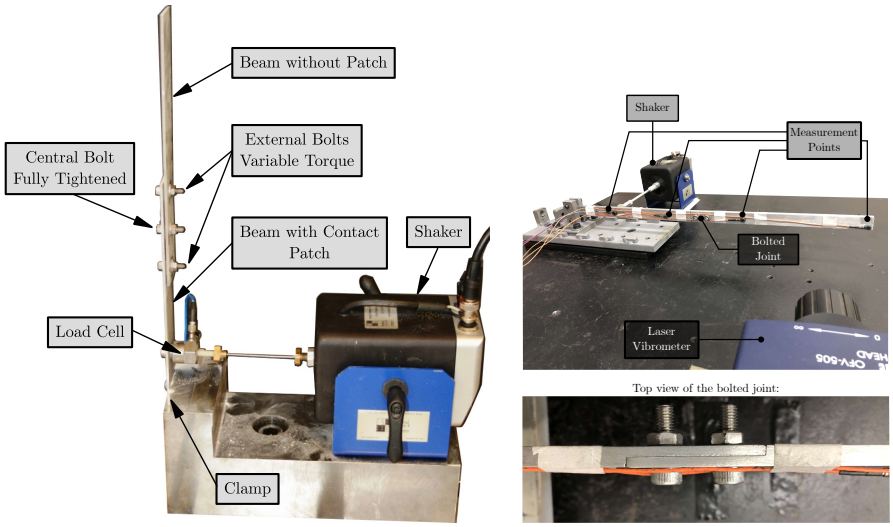

(a) Orion beam setup. (b) BERT setup.

Figure 1 – Experimental setup and the schematic representation illustrating the cantilever beam which carries a bolted joint connection.

is fully tightened with a torque of 80 cNm. A test is also performed considering the structure in its monolithic condition, i.e. the contact patches are glued together.

For this structure, the objective is to evaluate how the tightening torque values can influence its dynamic behavior, in particular, its capacity to damp the vibration response near the resonance frequencies as a result of friction dissipation. Previous studies have indicated that the 6th vibration mode is capable of providing greater indications of nonlinearity, since the stress imposed around the bolted joint is more pronounced. In order to isolate the vibration behavior of the 6th bending mode, step-sine tests were used, employing a strategy to control the excitation amplitude, such that it remains constant at the RMS level for the entire frequency range tested. The excitation force was controlled with the following RMS levels: $10, 50, 100, 150, 200$, and 250 mN.

Figure 2 depicts the nonlinear behavior of the Orion beam in the vicinity of the 6th bending mode for several tightening torque conditions and excitation amplitudes. Note that two mechanisms cause the frequency bandwidth to evolve: energy dissipation by friction and structure softening. Frictional energy dissipation leads to an asymptotic evolution of the vibration attenuation when full slip occurs. But this condition was never reached during testing. The loss of stiffness acts as a softening nonlinearity. It leads to the peak being laid down on the left and the bandwidth being widened if the damping is sufficient. If the damping is not sufficient concerning the softening effect, the bandwidth no longer increases and may even decrease. This happens with 20, 30, 80 cNm tightening torques above the 200 mN amplitude. When both increase simultaneously, the bandwidth increases continuously. This is the case for the 10 cNm torque.

Once properly isolated, the vibrating mode was approximated by the Duffing Van-der Pol model described by Eq. (1).

BERT benchmark

Figure 1(b) depicts the BoltEd stRucTure (BERT) benchmark[2]. The experimental setup consists of two aluminum beams assembled in a clamped-free boundary condition, each with dimensions of $270 \times 25.4 \times 6.35$ mm and connected by two M5 bolts, spaced along a length of 40 mm, with a tightening torque of 5 Nm. An electromagnetic Modal Shop 2400E shaker is placed at 85 mm from the clamped end to minimize shaker-structure interaction. All measurements were made at the free end of the assembled beam by a laser vibrometer Polytec OFV-525/5000S. The data acquisition was performed by an LMS SCADAS system. The input signals applied to excite the structure were conducted, assuming different voltage amplitude levels applied to the shaker amplifier, from low to high values (0.05, 0.10, 0.15, and 0.20 V).

This benchmark was initially used by Teloli et al. (2021a). Unlike the Orion beam, the interest behind this structure was to evaluate the ability of phenomenological models (Bouc-Wen model, for example) to describe experimental responses containing measurement variability and uncertainties, since the tests were conducted on different days. Not only that, the objective was also to verify the predictive ability of models to represent the vibration behavior of the structure in the transient regime through random tests (closer to real operating conditions of a structure), and also swept sine tests. Figure 3 exemplifies the data fluctuation considering several experimental measurements with 99% of statistical confidence bands and low (3(a)) and high (3(b)) excitation amplitudes for swept sine tests. It is in the context of these experimental tests that the GP-NARX model is identified.

[2]Data available on `https://github.com/shm-unesp/DATASET_BOLTEDBEAM`

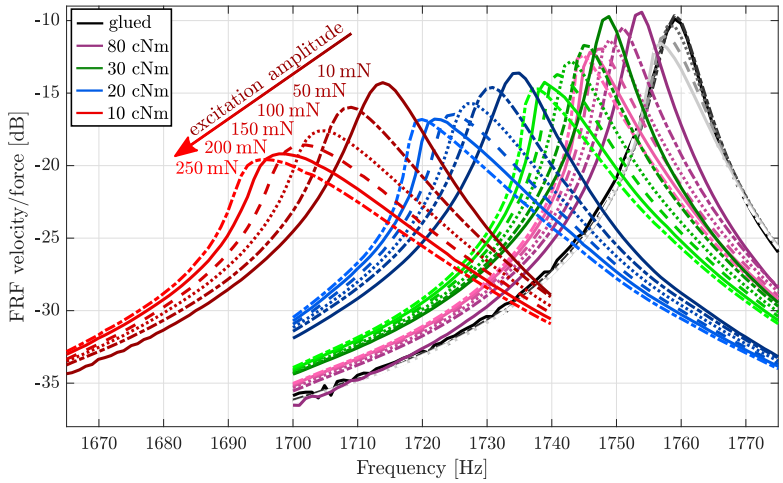

Figure 2 – Nonlinear behavior of the Orion lap-joint around 1665 and 1775 Hz for different torques (80 cNm, 30 cNm, 20 cNm, and 10 cNm) distinguished by different colors, and for multiple excitation level (10 mN to 250 mN) distinguished by different line types and gradient color. The greyscale curves show the behavior of a glued assembly.

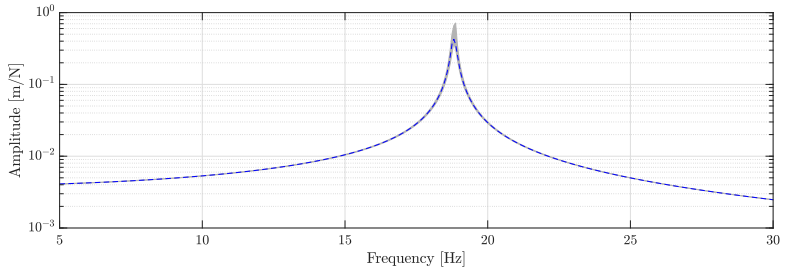

(a) Low level of excitation amplitude (0.05 V).

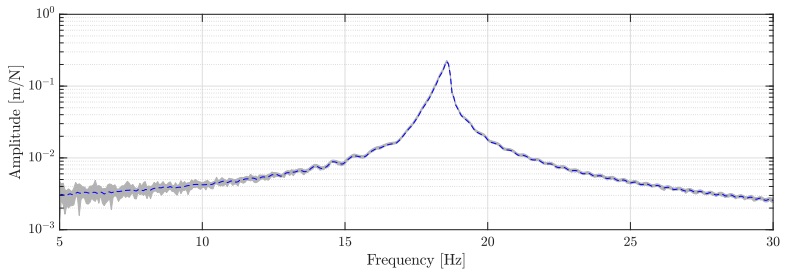

(b) High level of excitation amplitude (0.20 V).

Figure 3 – Variation of the Frequency Response Function calculated for different excitation amplitudes with 99% **of confidence bands. represents the confidence bands, whereas is the mean values.**

Evaluation of the Duffing-Van der Pol oscillator

Table 1 presents the set of parameters calibrated considering the glued condition, whereas Fig. 4 shows the evolution of calibrated parameters as a function of several tightening torque conditions. To emphasize the variations of m, c, k, α_n, and β_n when the preload varies, the identified values of glued condition (Table 1) are considered a reference and then used as normalization scale for other conditions.

Table 1 – Model parameters considering the glued condition for all excitation amplitudes.

m [kg]	c [Ns/m]	$k \times 10^7$ [N/m]	$\beta_n \times 10^{11}$ [Ns/m^3]	$\alpha_n \times 10^{15}$ [N/m^3]
0.0917	2.7946	1.1204	1.4862	-2.0090

Based on the estimated parameters, some indicators can be stressed out. On the one hand, note that the equivalent

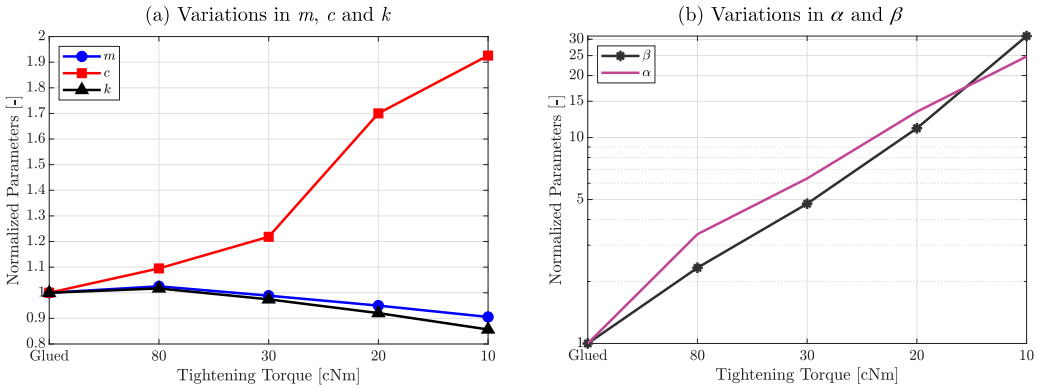

Figure 4 – Evolution of calibrated parameters as function of several tightening torque conditions.

coefficients of mass and stiffness are decreasing as a function of the tightening torque in Fig. 4(a). The formulation employed in equation 1 is equivalent to the representation of uncoupled reduced-order models, which is usually considered to describe full order Finite Element (FE) models but written on the physical basis. Notwithstanding the foregoing, the equivalent comparison can also be proposed: $m \equiv \Phi^T \mathbf{M} \Phi$ and $k \equiv \Phi^T \mathbf{K} \Phi$. Assuming the mass matrix constant, whereas the modal mass changes according to the applied torque level, one can note that the mode shapes change. The shape changes are small considering the numerical values and, therefore, validate assumptions made in previous numerical works, which consider that contact nonlinearities alter the mode shapes (Festjens et al., 2013). Additionally, the experimental tests used to calibrate the model were performed consecutively without disassembly of the setup. On the other hand, the equivalent damping coefficient almost doubled its value from the glued condition to the preload of 10 cNm, detaching that although m and k are sensitive to preload values changes, it is possible to increase damping, preserving the structural stiffness.

Figure 4(b) depicts the evolution of β_n and α_n for different torque values. These parameters are the projection of nonlinear forces that actuate in the 6th vibrating mode and show a significant increase in nonlinear terms' contribution to the structure's behavior for tightening torques far from the monolithic condition. Moreover, negative values of cubic stiffness α_n are expected once Fig. 2 indicates that the structure presents softening effects.

Figure 5 exhibits a comparison between the predicted frequency response curves for several torque conditions *versus* the experimental ones for a excitation level of 200 mN. Despite its simplicity, the Duffing-Van der Pol model proposed could reproduce with a satisfactory agreement with the experimental measurements.

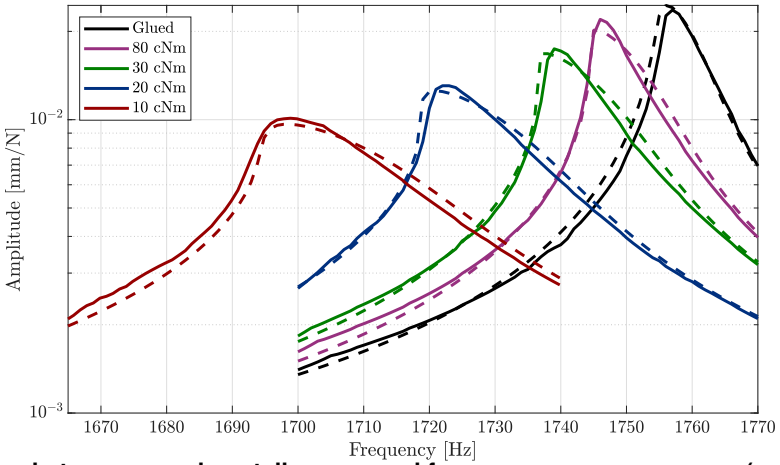

Figure 5 – Comparison between experimentally measured frequency response curves (solid lines ——)and the estimated ones by the Duffing-Van der Pol model (dashed lines — —).

Evaluation of the GP-NARX model

The identification workflow of the GP-NARX model may be stated as follows: (i) *Data acquisition:* For the training process of the GP-NARX model, swept sine tests in the resonance frequency vicinity were used to encode and reproduce nonlinearities of the BERT benchmark. Input and output data used for training were not used for model verification and validation; (ii) *Model training:* this step comprises the optimization of hyperparameters $\boldsymbol{\Theta}$ by maximizing the marginal log-likelihood from equation (18) and also the estimation of the maximum number of input/output lags. Notwithstanding,

data from different days are included into this step, to ensure that the model is able to take into account the variability observed in the Fig. 3; (iii) *Verification & validation:* this step is performed by considering *model predicted output*. Monte Carlo simulations are used to propagate all the model uncertainties, using the estimated Gaussian distribution.

Figure 6 depicts the model-predicted outputs with 99% of statistical confidence in direct comparison with experimental measurements when a level of 0.20 V (high excitation amplitude) is applied on the shaker amplifier. The confidence bands accommodate well the experimental responses, which indicates that the model can make accurate predictions of the structure's behavior and response, even in the presence of nonlinear effects. From these figures, note that the GP-NARX model can reproduce the dynamics of the BERT system even for capturing the hysteresis loop.

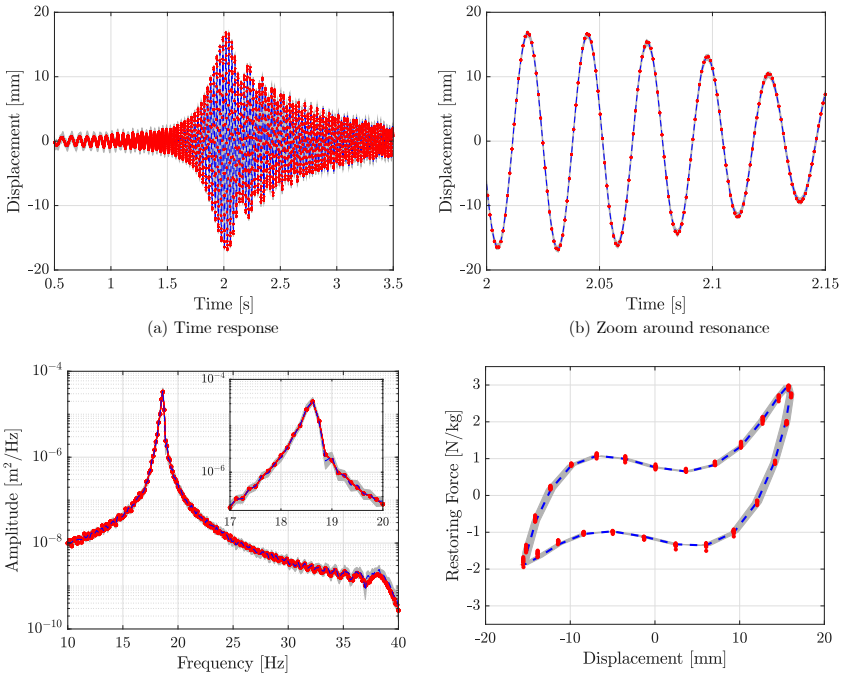

Figure 6 – Verification of the GP-NARX model for high excitation amplitude (0.20 V) considering a swept sine test. ▒ represents the 99% model-predicted output confidence bands, —— is the model response mean and • represents ten experimental realizations.

FINAL REMARKS

This paper presents the problem of identifying jointed structures from different points of view. One of the main advantages in the use of parametric models lies in the possibility of offering physical insight, through the identified model parameters, on the characteristics present in the real system. On the other hand, the model explored in this work is limited to applications involving isolated nonlinear vibration modes. Although the lack of physical parameters is one of the drawbacks in data-driven models, once identified, these models can provide features estimated directly from the data for decision making applications, such as detecting the presence of damage, or even information about the energy dissipated in systems with nonlinear damping (see the hysteresis loop present in Fig. 6(d), for example).

Future work will investigate the combined use of both approaches to form hybrid models: parametric models with physical insight will be used to represent measurable physical quantities such as strains, velocities, and accelerations. Complementarily, data-driven models will be integrated within this analysis of physics-based models to approximate physics that is hidden and cannot be directly measured, such as micro-displacements at the interface between regions of the bolted joint.

ACKNOWLEDGMENTS

The authors thank the financial support provided by Brazilian National Counsel of Technological and Scientific Development (CNPq) grant number 306526/2019-0 and São Paulo Research Foundation (FAPESP) grant numbers 16/21973-5 and 19/19684-3.

REFERENCES

Ewins, D. J., Weekes, B., and Delli CARRI, A. (2015). Modal testing for model validation of structures with discrete nonlinearities. *Philosophical Transactions of the Royal Society A: Mathematical, Physical and Engineering Sciences*,

373(2051):20140410.

Festjens, H., Chevallier, G., and Dion, J.-l. (2013). A numerical tool for the design of assembled structures under dynamic loads. *International Journal of Mechanical Sciences*, 75:170–177.

Gaul, L. and Nitsche, R. (2000). Friction control for vibration suppression. *Mechanical Systems and Signal Processing*, 14(2):139–150.

Jalali, H., Ahmadian, H., and Mottershead, J. E. (2007). Identification of nonlinear bolted lap-joint parameters by force-state mapping. *International Journal of Solids and Structures*, 44(25):8087 – 8105.

Miguel, L. P., Teloli, R. O., da Silva, S., and Chevallier, G. (2022). Probabilistic machine learning for detection of tightening torque in bolted joints. *Structural Health Monitoring*, 21(5):2136–2151.

Schulz, E., Speekenbrink, M., and Krause, A. (2018). A tutorial on Gaussian process regression: Modelling, exploring, and exploiting functions. *Journal of Mathematical Psychology*, 85:1 – 16.

Seeger, M. (2004). Gaussian Process for Machine Learning. *International Journal of Neural Systems*, 14(02):69–106.

Teloli, R. O., Butaud, P., Chevallier, G., and da Silva, S. (2022). Good practices for designing and experimental testing of dynamically excited jointed structures: The orion beam. *Mechanical Systems and Signal Processing*, 163:108172.

Teloli, R. O., da Silva, S., Ritto, T. G., and Chevallier, G. (2021a). Bayesian model identification of higher-order frequency response functions for structures assembled by bolted joints. *Mechanical Systems and Signal Processing*, 151:107333.

Teloli, R. O., Villani, L. G., da Silva, S., and Todd, M. D. (2021b). On the use of the gp-narx model for predicting hysteresis effects of bolted joint structures. *Mechanical Systems and Signal Processing*, 159:107751.

Williams, C. K. I. and Rasmussen, C. E. (2006). *Gaussian processes for machine learning*, volume 2. MIT Press Cambridge, MA, Cambridge.

RESPONSIBILITY NOTICE

The authors are the only responsible for the printed material included in this paper.